Chinese Chemical Letters 35 (2024) 108928

Contents lists available at ScienceDirect

Chinese Chemical Letters

journal homepage: www.elsevier.com/locate/cclet

Nanomedicine integrating the lipidic derivative of 5-fluorouracil, miriplatin and PD-L1 siRNA for enhancing tumor therapy

An Lu[a,1], Yuhao Guo[a,1], Yi Yan[a,1], Lin Zhai[a], Xiangyu Wang[a], Weiran Cao[b], Zijie Li[c], Zhixia Zhao[d], Yujie Shi[a], Yuanjun Zhu[a], Xiaoyan Liu[a], Huining He[b], Zhiyu Wang[c], Jian-Cheng Wang[a,e,*]

[a] *Beijing Key Laboratory of Molecular Pharmaceutics and New Drug Delivery Systems, State Key Laboratory of Natural and Biomimetic Drugs, School of Pharmaceutical Sciences, Peking University, Beijing 100191, China*
[b] *Tianjin Key Laboratory on Technologies Enabling Development of Clinical Therapeutics and Diagnostics, School of Pharmacy, Tianjin Medical University, Tianjin 300070, China*
[c] *Department of Immuno-oncology, The Fourth Hospital of Hebei Medical University, Shijiazhuang 050011, China*
[d] *Department of Pharmacy, Clinical Trial Research Center, China-Japan Friendship Hospital, Beijing 100029, China*
[e] *Laboratory of innovative formulations and pharmaceutical excipients, Ningbo Institute of Marine Medicine, Peking University, Ningbo 315832, China*

ARTICLE INFO

Article history:
Received 8 May 2023
Revised 2 August 2023
Accepted 9 August 2023
Available online 12 August 2023

Keywords:
Chemo-immunotherapy
Immune checkpoint inhibition
Gene silencing
Miriplatin
Macrophage phagocytosis
Nanotechnology

ABSTRACT

Immunosuppressive microenvironments present critical problems in clinical chemotherapy. To regulate the tumor immune microenvironment for enhancing antitumor effect, a combination of immune checkpoint inhibitors (ICIs) with chemotherapeutics has been applied clinically. In this study, miriplatin (MiPt), the lipidic derivative of 5-fluorouracil (Fu-OA), as well as the programmed death ligand 1 (PD-L1) target siRNA (siPD-L1) were integrated into Lip-Pt/Fu@siPD-L1 nanoparticles (NPs) for chemo-immunotherapy. *In vitro* results showed that Lip-Pt/Fu@siPD-L1 NPs could exhibit effective siRNA gene silencing and promote the phagocytosis of tumor cells by macrophages. Furthermore, *in vivo* results revealed that Lip-Pt/Fu@siPD-L1 NPs showed significantly higher anti-tumor efficiency than that of the physical mixing of MiPt, 5-fluorouracil, and Lip@siPD-L1 NPs (delivery of siPD-L1 by liposomes). The best anti-tumor efficiency of Lip-Pt/Fu@siPD-L1 NPs resulted from the synergistic immunotherapeutic effects of MiPt and siPD-L1 based on the inhibition of CD47 expression and the downregulation of PD-L1 in tumor cells, which elicited a robust anti-tumor immune response through the activation of macrophage phagocytosis and immune checkpoint inhibition. The Lip-Pt/Fu@siPD-L1 NPs provide a potential strategy for tumor chemo-immunotherapy.

Many studies have shown that the pathogenesis and progression of tumors are related to an extremely complex protein network system [1,2]. Single-target treatment strategies are often insufficient to inhibit tumor progression [3,4]. Multi-drug combination chemotherapy has gradually become the mainstream [5,6]. For example, the XELOX regimen, including oxaliplatin and capecitabine, is commonly used as a first-line chemotherapy for gastrointestinal carcinoma [7]. However, clinical studies have reported that the up-regulation of programmed death-ligand 1 (PD-L1) expression commonly occurs in tumor patients after chemotherapy, which aggravates the inhibitory immune microenvironment [8]. Therefore, aiming to solve the problem of the immunosuppressive microenvironments is becoming an important aim in research related to improving chemotherapy.

In recent years, neutralizing inhibitory immune checkpoint signaling proteins such as programmed cell death protein 1 (PD-1) and its ligand *via* immune checkpoint inhibitors (ICIs) has provided an effective strategy to inhibit the tumor progression [9,10]. The strategy of combining ICIs with traditional chemotherapeutics has achieved significant results in clinical practice, as well as preclinical research [11]. For instance, the result of KEYNOTE-590 (NCT03189719) trial showed that pembrolizumab (*i.v.*) plus 5-fluorouracil (5-Fu, *i.v.*) and cisplatin (*i.v.*) has more benefits than the combination of 5-Fu and cisplatin, as a first-line regimen for the treatment of advanced esophageal cancer [12]. Platinum drugs, such as cisplatin, carboplatin, oxaliplatin, are widely used as chemotherapy agents clinically [13,14]. Interestingly, different platinum drugs have different immune regulatory effects [15,16]. For

* Corresponding author.
E-mail address: wang-jc@bjmu.edu.cn (J.-C. Wang).
[1] These authors contributed equally to this work.

https://doi.org/10.1016/j.cclet.2023.108928
1001-8417/

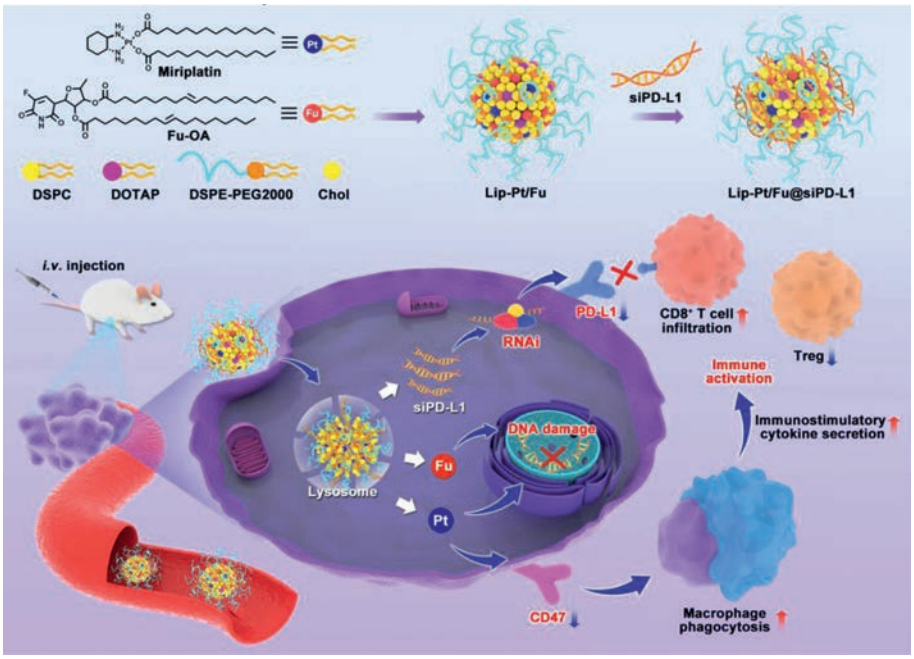

Scheme 1. Schematic illustration of the composition of Lip-Pt/Fu@siPD-L1 nanomedicine and the synergistic anti-tumor mechanisms.

example, oxaliplatin induces immunogenic cell death (ICD) to reprogram immunosuppressive tumor microenvironments, which enhances the immunotherapeutic effect with ICIs [17,18]. The combination of different platinum drugs and ICIs would prove advantageous in tumor treatment due to their synergistic anti-tumor mechanisms. Miriplatin (MiPt, an analog of oxaliplatin) has been approved to treat hepatocellular carcinoma (HCC) by transcatheter arterial chemoembolization in Japan [19,20]. Up to now, the combined application of MiPt with ICIs and their synergistic immune mechanisms have not been reported.

Although the combination strategies of chemotherapeutics and ICIs have achieved better patient survival rates, it has not achieved its optimal efficiency because of the unresolved pharmacokinetic defects of each drug [21]. Nanotechnology provides great advantages in the treatment of malignant tumor through prolonging the blood circulation time of drugs, and increasing both tumor accumulation and cellular uptake of drugs [22,23]. It was shown that the integrated delivery of multiple drugs not only improves the pharmacokinetics of the transported drugs, but also results in better synergistic anti-tumor efficacy of multiple drugs [24,25].

Herein, we designed a lipid-based nanoparticle platform to co-deliver MiPt, the lipidic derivative of 5-Fu (Fu-OA), and the PD-L1 target siRNA (siPD-L1) for synergistic chemo-immunotherapy. Lipophilic MiPt is easy to assemble with phospholipids to form liposomes. The Fu-OA was obtained by conjugating doxifluridine with hydrophobic oil acid tail chains, which was benefit to be assembled into liposomes. Also, siPD-L1 was condensed in the liposomal nanoparticles with cationic 1,2-dioleoyl-3-trimethylammonium-propane (DOTAP) lipid materials. As shown in Scheme 1, Lip-Pt/Fu@siPD-L1 nanoparticles (NPs) contained MiPt and Fu-OA inserted into the lipid layer, and siPD-L1 loaded by electrostatic interaction. After cellular uptake of Lip-Pt/Fu@siPD-L1 NPs, MiPt and Fu-OA induced cytotoxicity through DNA damage and cell cycle arrest, respectively. Then, an anti-tumor immune response was activated by promoting macrophage phagocytosis of tumor cells with CD47 expression inhibition by MiPt. Finally, with the downregulation of PD-L1 by siRNA, the macrophage-based anti-tumor immune response dramatically augmented anti-tumor T-cell immunity.

The Fu-OA was synthesized as described in Fig. S1 (Supporting information). The structure of Fu-OA was confirmed using nuclear magnetic resonance (NMR) spectrometry (Figs. S2 and S3 in Supporting information) and electrospray ionization-mass spectrometry (ESI-MS) (Fig. S4 in Supporting information). The preparation of Lip-Pt/Fu@siRNA NPs was performed with thin-film hydration method and the siRNA was loaded by electrostatic interaction. As shown in Fig. 1A and Fig. S5 (Supporting information), the uniform Lip-Pt/Fu@siRNA NPs with an average diameter of 179.8 nm, the polydispersity index (PDI) of 0.2376 and the zeta potential of 39.74 mV were verified using dynamic light scattering (DLS). Scanning electron microscope (SEM) imaging revealed that the Lip-Pt/Fu@siRNA NPs possessed a spherical shape (Fig. 1B). The result of gel retardation assay showed that the siRNA could be completely encapsulated in the Lip-Pt/Fu@siRNA NPs at a N/P = 27/1 (Fig. 1C), and released after mixing with Triton X-100 (Fig. 1D). The drug loading of MiPt and Fu-OA is 50 and 100 μg/mg, respectively. The stability of siRNA in Lip-Pt/Fu@siRNA NPs in serum was also proved using gel retardation assay (Fig. S6 in Supporting information). Compared with free siRNA, the encapsulated siRNA in Lip-Pt/Fu@siRNA NPs could keep intact structures up to 48 h in incubation with serum at 37 °C. As shown in Fig. S7A (Supporting information), there was no significant change in particle size when the Lip-Pt/Fu@siRNA NPs were kept at 4 °C for 30 days. The Lip-Pt/Fu@siRNA NPs could remain a stable particle size of under 200 nm even after 128-fold dilution by 5% glucose solution (Fig. S7B in Supporting information).

It is necessary to inhibit tumor progression by multi-target anti-tumor drugs combined with different action pathways and mechanisms [26]. The half maximal inhibitory concentration (IC_{50}) was calculated using the 3-(4,5-dimethylthiazol-2-yl)−2,5-diphenyltetrazolium bromide (MTT) assay. As shown in Fig. 1E, Fu-OA (IC_{50} = 53.04 μmol/L) and 5-Fu (IC_{50} = 64.20 μmol/L) showed equivalent cytotoxicity against CT26 cells. Moreover, the IC_{50} value of MiPt against CT26 cells was 98.33 μmol/L, while a higher cyto-

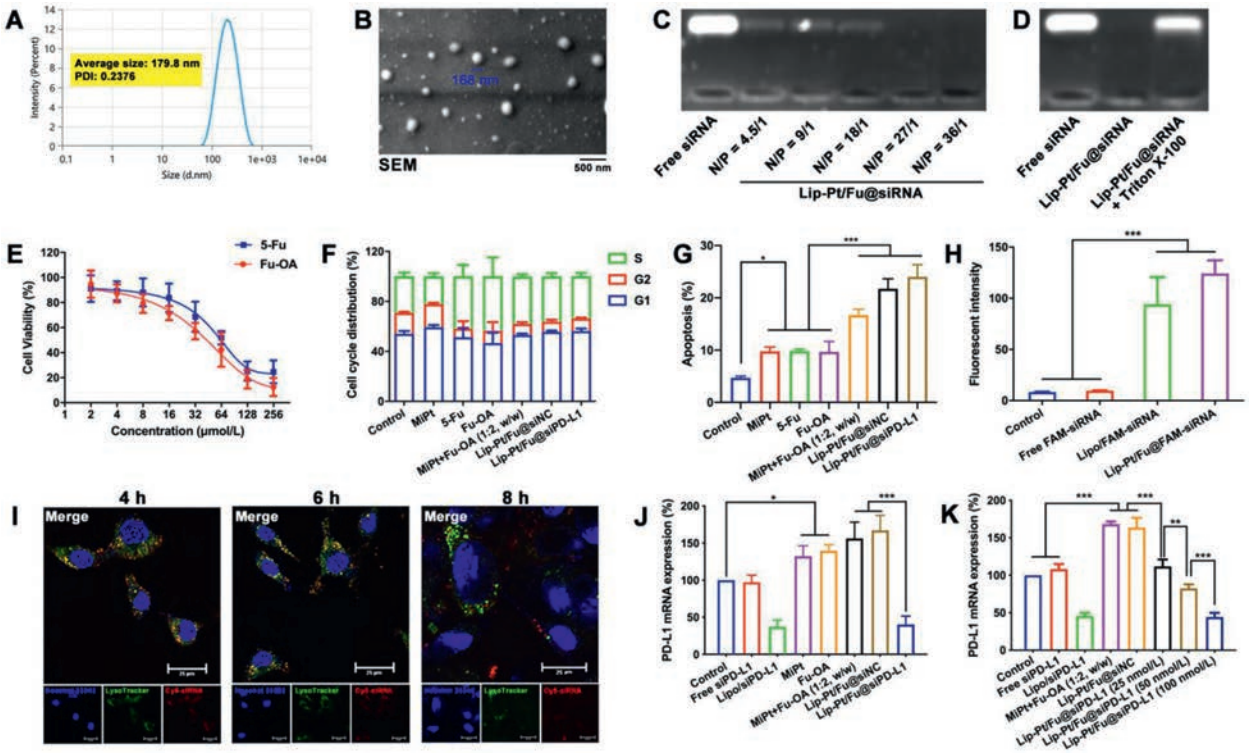

Fig. 1. The *in vitro* anti-tumor mechanisms and siRNA transfection efficiency of Lip-Pt/Fu@siPD-L1 NPs in CT26 cells. (A) The size of Lip-Pt/Fu@siRNA NPs. (B) The SEM image of Lip-Pt/Fu@siRNA NPs. Scale bar = 500 nm. (C) The siRNA loading efficiency of Lip-Pt/Fu@siRNA NPs with different N/P ratios. (D) siRNA released from Lip-Pt/Fu@siRNA NPs after mixing with Triton X-100. (E) Cytotoxicity profiles of 5-Fu and Fu-OA against CT26 cells. (F) Cell cycle distribution of CT26 cells after treatment with different formulations ($n = 3$). (G) Apoptosis analysis of CT26 cells by Annexin V/PI staining after treatment with different formulations ($n = 3$). (H) Intracellular fluorescence intensity detected using flow cytometry after treatment with Lip-Pt/Fu@FAM-siRNA NPs in CT26 cells ($n = 3$). (I) Confocal imaging of co-localization (yellow) of Lip-Pt/Fu@Cy5-siRNA NPs (red) with lysosomes (stained with LysoTracker Red DND-99, green) in CT26 cells. The nucleus was stained with Hoechst 33342 (blue). Scale bar = 25 μm. (J) The relative expression levels of PD-L1 mRNA detected using qRT-PCR in CT26 cells after treatment with different formulations ($n = 6$). (K) The relative expression levels of PD-L1 mRNA detected using qRT-PCR in CT26 cells after treatment with gradient concentration of siPD-L1 in Lip-Pt/Fu@siPD-L1 NPs ($n = 3$). Data represent mean ± standard deviation (S.D.). $^{*}P < 0.05$, $^{**}P < 0.01$, and $^{***}P < 0.001$.

toxicity ($IC_{50} = 14.88$ μmol/L) was observed when combined with Fu-OA (1:2, w/w). Also, a higher cytotoxicity ($IC_{50} = 29.38$ μmol/L) of Fu-OA was observed when combined with MiPt (Figs. S8A and B in Supporting information). The combination index (CI) was used to indicate the synergism between two drugs. It was worth noting that the CI of MiPt and Fu-OA combination (1:2, w/w) against CT26 cells was 0.71, displaying superior synergetic effect. The IC_{50} values of MiPt and Fu-OA encapsulated in Lip-Pt/Fu@siPD-L1 NPs were 11.76 and 23.22 μmol/L, respectively (Fig. S8C in Supporting information). As shown in Fig. 1F and Fig. S9 (Supporting information), flow cytometry was used to analyze the cell cycle distribution of CT26 cells after treatment with Fu-OA and Lip-Pt/Fu@PD-L1 NPs. Compared with the control group, Fu-OA and 5-Fu both resulted in cell cycle arrest at the S phase, which indicates that Fu-OA has a similar anti-tumor mechanism to 5-Fu. Moreover, MiPt slightly arrested the cell cycle at the G1 phase. The cell cycle arrested by Lip-Pt/Fu@PD-L1 NPs occurred at both the S phase and the G1 phase, which was similar to Lip-Pt/Fu NPs and Lip-Pt/Fu@siNC NPs (loading negative control siRNA). Therefore, the effect of Lip-Pt/Fu@PD-L1 NPs on cell cycle arrest was attributed to MiPt and Fu-OA, not siPD-L1.

γH2AX, the phosphorylation of H2AX on the S139 site, is a sensitive marker of DNA damage response and DNA double-strand breaks repair [1]. Enzyme linked immunosorbent assay (ELISA) was used to detect the expression of γH2AX protein in CT26 cells after treatment with Lip-Pt/Fu@PD-L1 NPs. As shown in Fig. S10 (Supporting information), compared with the control group, MiPt and Fu-OA showed increased γH2AX expression because of the formation of Pt-DNA adducts and cell cycle arrest, respectively. When treated with Lip-Pt/Fu@PD-L1 NPs, the expression of γH2AX protein in CT26 cells was also significantly increased, which was similar to that of the combination of MiPt and Fu-OA (1:2, w/w) as well as Lip-Pt/Fu@siNC NPs. To test whether Lip-Pt/Fu@siPD-L1 NPs could activate apoptosis, CT26 cells were co-stained with Annexin-V-fluorescein isothiocyanate (FITC) and propidium iodide (PI) after treatment with Lip-Pt/Fu@siPD-L1 NPs, and the number of apoptotic cells (including the early and late apoptosis) was estimated using flow cytometry. As shown in Fig. 1G and Fig. S11 (Supporting information), compared with the control group (4.7%), Lip-Pt/Fu@siPD-L1 NPs exhibited the highest apoptosis induction rate of 24.0%, in contrast to 9.8% related to MiPt, 9.8% related to 5-Fu, 9.7% related to Fu-OA, 16.7% related to MiPt plus Fu-OA (1:2, w/w), and 21.7% related to Lip-Pt/Fu@siNC NPs. In summary, Lip-Pt/Fu@siPD-L1 NPs activated powerful apoptotic effects based on the mechanisms of DNA damage and cell cycle arrest.

Efficient cellular internalization and lysosomal escape are the key steps for siRNA delivery to achieve target gene silencing [27]. As shown in Fig. S12 (Supporting information), fluorescence imaging using confocal laser scanning microscope (CLSM) showed that the Lip-Pt/Fu@FAM-siRNA NPs exhibited high cellular uptake efficiency similar to that of the commercial transfection reagent Lipo/FAM-siRNA in CT26 cells. This was consistent with the results of flow cytometry (Fig. 1H). To further investigate whether siRNA-loaded NPs could escape from endosomes/lysosomes following cellular uptake, intracellular fluorescence distribution was observed using CLSM. As shown in Fig. 1I, most of co-localized fluo-

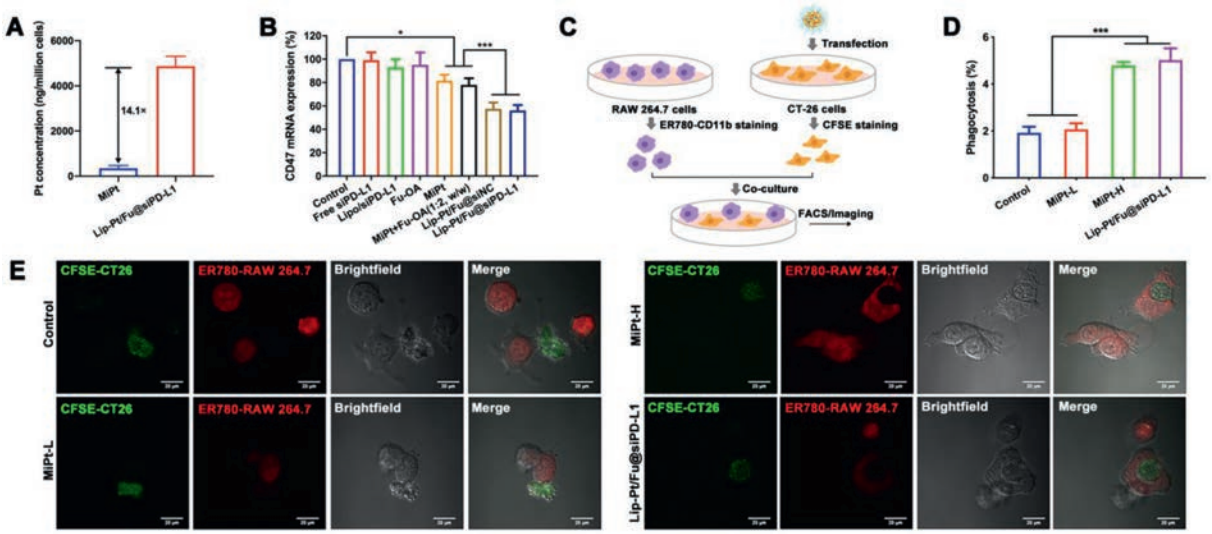

Fig. 2. Promoting macrophage phagocytosis by inhibition of CD47 expression on tumor cells. (A) The accumulation of Pt in CT26 cells after treatment with MiPt and Lip-Pt/Fu@siPD-L1 NPs ($n = 3$). (B) The mRNA expression of CD47 detected using qRT-PCR in CT26 cells after treatment with different formulations ($n = 5$). (C) Schematic illustration of the design of *in vitro* phagocytosis assay. After treatment of Lip-Pt/Fu@siPD-L1 NPs, CT26 cells were stained by CFSE and co-incubated with anti-mouse CD11b antibody (ER780)-stained RAW 264.7 cells for 6 h. (D) Phagocytosis ratio of CT26 cells was determined using flow cytometry ($n = 3$). (E) Confocal imaging of CFSE-stained CT26 cells (green) phagocytosed by ER780-stained RAW 264.7 cells (red). Scale bar = 20 μm. Data represent mean ± S.D. $^{*}P < 0.05$, $^{***}P < 0.001$.

rescence dots (yellow) were observed in the cytoplasm of the CT26 cells after treatment with Lip-Pt/Fu@Cy5-siRNA NPs for 4 or 6 h. This revealed that most of NPs (red) were trapped in the lysosomes (green). Meanwhile, a larger proportion of red fluorescence dots were separated from the green fluorescence dots after 8 h of incubation, which demonstrated that siRNA could be released from lysosomes. In order to further accurately evaluate the PD-L1 downregulation efficacy of Lip-Pt/Fu@siPD-L1 NPs, quantitative real time polymerase chain reaction (qRT-PCR) and Western blot were used to investigate the siPD-L1 silencing effects on mRNA and protein levels in tumor cells, respectively. As shown in Fig. 1J, MiPt, Fu-OA, the formulation of MiPt plus Fu-OA (1:2, w/w) and Lip-Pt/Fu@siNC NPs all significantly up-regulated the expression of PD-L1 mRNA in CT26 cells compared with the control group. This indicated that chemotherapy, based on MiPt and Fu-OA, exerted the negative immunomodulation. Surprisingly, a significant 76.0% down-regulation rate of PD-L1 mRNA expression in CT26 cells was observed after treating cells with Lip-Pt/Fu@siPD-L1 NPs. The expression levels of PD-L1 proteins detected using Western blot (Fig. S13 in Supporting information) were consistent with the results of qRT-PCR. The gene silencing effect of Lip-Pt/Fu@siPD-L1 NPs on PD-L1 mRNA was dose-dependent (Fig. 1K). Based on the above results, Lip-Pt/Fu@siPD-L1 NPs exhibited an excellent gene silencing effect, which was attributed to the efficient cellular internalization and lysosomal escape.

The concentrations of Pt in CT26 cells treated with free MiPt and Lip-Pt/Fu@PD-L1 NPs were assessed using inductively coupled plasma-mass spectrometry (ICP-MS). Interestingly, in the Lip-Pt/Fu@PD-L1 NPs group, the concentration of Pt (4872.1 ng/million cells) were 14.1-fold higher than that in the free MiPt group (345.2 ng/million cells) (Fig. 2A). In addition, the expression level of CD47 in CT26 cells was measured using qRT-PCR and Western blot. As shown in Fig. 2B, free siPD-L1, lipo/siPD-L1 and Fu-OA showed zero influence on the expression of CD47 mRNA in CT26 cells. Compared with the control group, 18.3% of CD47 mRNA expression was downregulated in the MiPt group, similar as the formulation of MiPt plus Fu-OA. Stronger than that of MiPt, 42.4% and 43.8% of CD47 mRNA expression in Lip-Pt/Fu@siNC NPs and Lip-Pt/Fu@siPD-L1 NPs were downregulated, respectively. This can be attributed to the higher MiPt accumulation in CT26 cells. The expression of CD47 protein tested by Western blot (Fig. S14 in Supporting information) was coincided with the results of qRT-PCR.

To further evaluate the influence of CD47 inhibition on macrophage phagocytosis, the phagocytosis index was analyzed using flow cytometry and the phagocytosis behavior was observed using CLSM. As shown in Fig. 2C, after treated with Lip-Pt/Fu@siPD-L1 NPs, the CT26 cells were stained by carboxyfluorescein diacetate succinimide ester (CFSE), and then co-incubated with RAW 264.7 cells (a classical murine macrophage) stained with anti-mouse CD11b antibody (ER780) for 6 h, and the phagocytosis index was calculated as the ratio of the CFSE/ER780 double positive cells. As shown in Fig. 2D and Fig. S15 (Supporting information), compared with the control group (1.92%), the phagocytosis index in Lip-Pt/Fu@siPD-L1 NPs group (equivalent to 15 μg/mL MiPt) increased to 5.02%, which was similar to that of the high-dose MiPt group (MiPt-H, 200 μg/mL). While, the low-dose MiPt group (MiPt-L, 15 μg/mL) exerted nearly no influence on the phagocytosis index. This trend of increased phagocytosis of Lip-Pt/Fu@siPD-L1 NPs was attributed to its CD47 inhibition effects. As shown in Fig. 2E, CT26 cells treated with MiPt-H and Lip-Pt/Fu@siPD-L1 NPs were efficiently engulfed by the macrophages, while the CT26 cells treated with MiPt-L were not, indicating that efficient CD47 inhibition could promote the phagocytosis of tumor cells by macrophages.

The pharmacokinetic studies were performed in BALB/c mice after intravenous injection of Lip-Pt/Fu@siPD-L1 NPs. As shown in Figs. 3A–C and Tables S1–S3 (Supporting information), compared with the free drugs, significant prolonged distribution half-life ($t_{1/2\alpha}$) values of Cy5-siRNA (0.216 h *vs.* 1.220 h) and Pt (0.144 h *vs.* 0.872 h) were found in the Lip-Pt/Fu@Cy5-siRNA NPs group and the Lip-Pt/Fu@siPD-L1 NPs group. Moreover, their corresponding area under the plasma concentration-time curve from time zero to infinity ($AUC_{0\rightarrow inf}$) values were increased by 5.9 and 4.1-fold, respectively. In addition, the $t_{1/2\alpha}$ value of Fu-OA in NPs was 2.023 h. The improved pharmacokinetic profiles of siRNA, Pt, and Fu-OA by the PEGylated NPs benefit *in vivo* drug accumulation within tumor tissues.

Furthermore, the fluorescence biodistribution of Cy5-siRNA in Lip-Pt/Fu@siRNA NPs was performed using *in vivo* imaging after intravenous injection in BALB/c mice with CT26-bearing heterotopic tumors, free Cy5-siRNA was used as the control group (Fig. S16 in

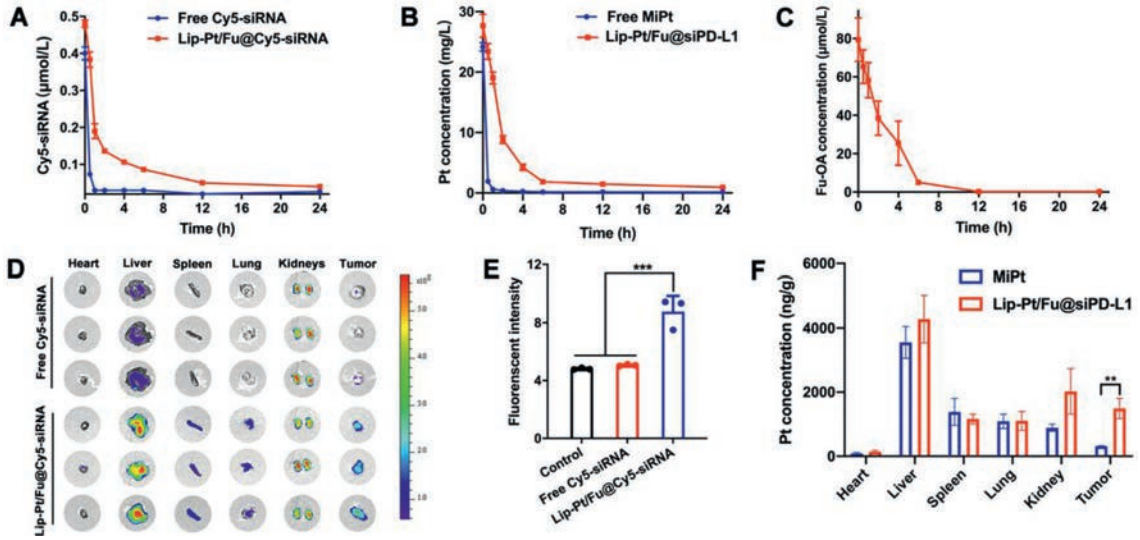

Fig. 3. Pharmacokinetics and biodistribution. (A) Time-dependent Cy5-siRNA concentrations in the blood of BALB/c mice after an *i.v.* dose of free Cy5-siRNA or Lip-Pt/Fu@Cy5-siRNA NPs ($n = 3$). (B) Time-dependent Pt concentrations in the blood of BALB/c mice after an *i.v.* dose of MiPt or Lip-Pt/Fu@siPD-L1 NPs ($n = 3$). (C) Time-dependent Fu-OA concentrations in the blood of BALB/c mice after an *i.v.* dose of Lip-Pt/Fu@siPD-L1 NPs ($n = 3$). (D) *Ex vivo* imaging of resected organs (heart, liver, spleen, lung, and kidneys) and tumor tissue from CT26-bearing heterotopic tumor models after *i.v.* of Cy5-siRNA or Lip-Pt/Fu@Cy5-siRNA NPs for 6 h ($n = 3$) (Radiant Efficiency $\times 10^8$: $(p/sec/cm^2/sr)/(\mu W/cm^2)$). (E) Intracellular fluorescence intensity of tumor cells from CT26-bearing heterotopic tumor models detected using flow cytometry after *i.v.* of Cy5-siRNA or Lip-Pt/Fu@Cy5-siRNA NPs for 6 h ($n = 3$). (F) Pt biodistribution after *i.v.* of MiPt or Lip-Pt/Fu@siPD-L1 NPs to CT26-bearing heterotopic tumor models for 6 h ($n = 3$). Data represent mean ± S.D. $^{**}P < 0.01$, $^{***}P < 0.001$.

Supporting information). The results showed that the fluorescence intensity of free Cy5-siRNA was quickly cleared at the 8 h point after injection, while the fluorescence intensity of Lip-Pt/Fu@Cy5-siRNA NPs remained to be clearly observed in the tumor tissue at the 48 h point after injection. This observation was further supported by *ex vivo* imaging of major tissues (heart, liver, spleen, lung, kidneys, and tumor) harvested 6 h post injection. As shown in Fig. 3D, a pronounced fluorescence intensity of Cy5-siRNA could be observed in tumor tissues treated with Lip-Pt/Fu@Cy5-siRNA NPs, while free Cy5-siRNA hardly accumulated within the tumor tissues. Moreover, compared with the free Cy5-siRNA group, a significantly higher intracellular fluorescence intensity of Lip-Pt/Fu@Cy5-siRNA NPs in the separated cells after tissue homogenate could also be observed using flow cytometry at 6 h point after injection (Fig. 3E). For *in vivo* distribution of Pt, ICP-MS was used to measure the concentration of Pt in major tissues (heart, liver, spleen, lung, kidneys, and tumor). As shown in Fig. 3F, at 6 h point after injection of Lip-Pt/Fu@siRNA NPs, the concentration of Pt in tumor tissues was 4.7-fold higher than that of free MiPt. The above results suggested that Lip-Pt/Fu@siRNA NPs could be enriched in tumor tissues by the enhanced permeability and retention (EPR) effect.

As shown in Fig. 4A, on day 7 after tumor inoculation, the tumor volume reached approximate 50 mm^3, and the BALB/c mice with CT26-bearing heterotopic tumor were randomly divided to seven groups and injected intravenously with 5% glucose solution, MiPt, the formulation of MiPt plus 5-Fu, the formulation of MiPt plus 5-Fu plus free siPD-L1, the formulation of MiPt plus 5-Fu plus Lip@siPD-L1 NPs (cationic liposomes delivering siPD-L1), Lip-Pt/Fu@siNC NPs, and Lip-Pt/Fu@siPD-L1 NPs every three days, respectively. All animal care and experiments were approved by the Institutional Authority for Laboratory Animal Care of Peking University. Among the groups, the most potent anti-tumor effect was observed in the Lip-Pt/Fu@siPD-L1 NPs group (Figs. 4B and C). It was noteworthy that the anti-tumor effect of Lip-Pt/Fu@siPD-L1 NPs was significantly higher than the formulation of MiPt plus 5-Fu plus free siPD-L1 (or Lip@siPD-L1), which revealed that the "three-in-one" integrated delivery strategy performed better than that of the physical mixing. Compared with the Lip-Pt/Fu@siNC NPs, Lip-Pt/Fu@siPD-L1 NPs exerted better anti-tumor efficacy due to siPD-L1 gene silencing effect. The expression of Bcl-2, as an anti-apoptotic factor, was detected using qRT-PCR in mRNA level to evaluate the apoptosis of tumor cells (Fig. S17 in Supporting information), and the results were coincided with the tumor growth inhibitory effect. The anti-tumor efficacy of all treatment groups was further confirmed using hematoxylin and eosin (H&E) staining (Fig. S18A in Supporting information) and terminal deoxynucleotidyl transferase dUTP nick-end labeling (TUNEL) assay (Fig. S18B in Supporting information). All treatment groups showed varying degrees of necrosis and apoptosis in tumor tissues, with the most significant effect in the Lip-Pt/Fu@siPD-L1 NPs group.

To further evaluate the anti-tumor mechanisms of Lip-Pt/Fu@siPD-L1 NPs, the expression of PD-L1 and CD47 in tumor tissues were detected using qRT-PCR and Western blot. As shown in Fig. 4D, MiPt, the formulation of MiPt plus 5-Fu, the formulation of MiPt plus 5-Fu plus free siPD-L1, and Lip-Pt/Fu@siNC NPs all up-regulated the expression of PD-L1 mRNA in the tumor tissues when compared with the control group. Interestingly, both of the Lip-Pt/Fu@siPD-L1 NPs and the formulation of MiPt plus 5-Fu plus Lip-siPD-L1 significantly down-regulated the expression of PD-L1 mRNA in the tumor tissues due to their effective delivery of siPD-L1. As shown in Fig. 4E, compared with the control group, the expression of CD47 in the tumor tissues from other groups was inhibited. This was attributed to the effect of MiPt. A stronger CD47 inhibition was observed in the Lip-Pt/Fu@siNC NPs and Lip-Pt/Fu@siPD-L1 NPs group than other groups, due to their higher intratumoral accumulation of Pt. The expression levels of PD-L1 and CD47 protein in the tumor tissues detected using Western blot (Fig. 4F) were consistent with the results of qRT-PCR. To understand the immune mechanisms underlying the superior therapeutic effect of Lip-Pt/Fu@siPD-L1 NPs, the immune cell populations were analyzed using flow cytometry. The gating strategy of cell sorting was shown in Figs. S19–S21 (Supporting information). As shown in Fig. S22A (Supporting information), compared with the control group (18.30%), the proportion of tumor-infiltrating $CD8^+$ T cells from the tumor tissues treated with the formulations of MiPt (23.86%), MiPt plus 5-Fu (24.53%) and MiPt plus 5-Fu plus

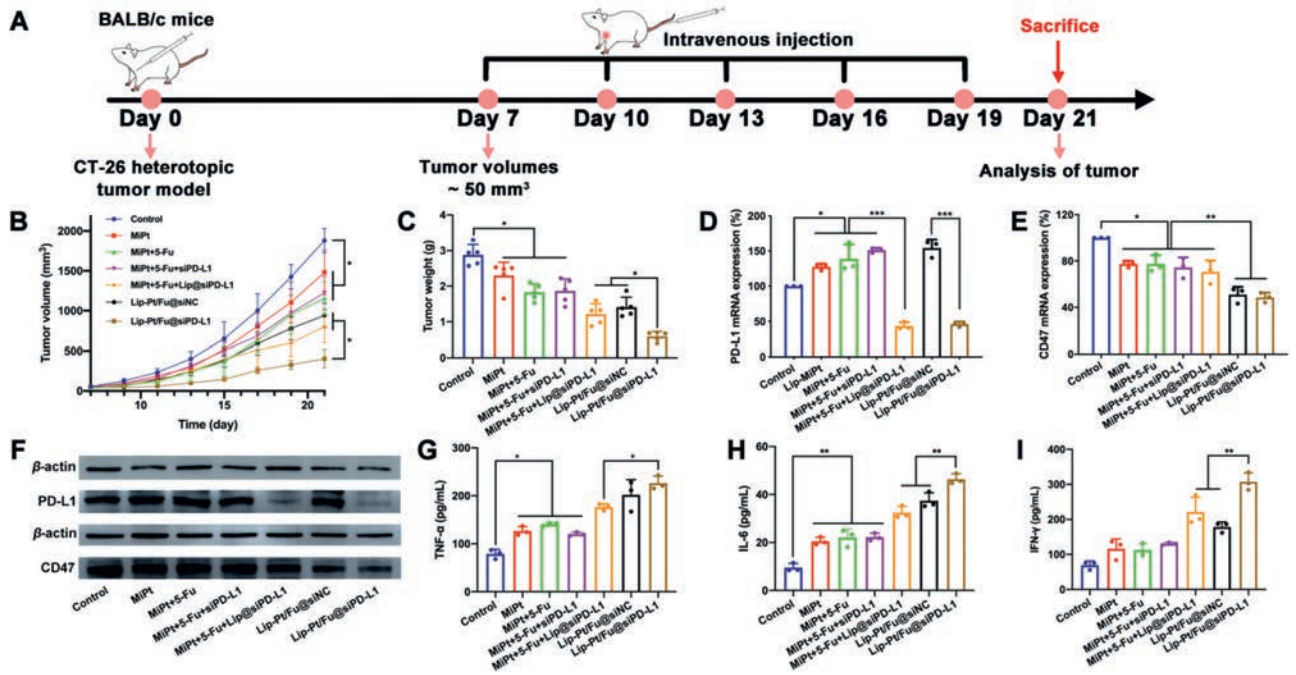

Fig. 4. *In vivo* anti-tumor efficacy of Lip-Pt/Fu@siPD-L1 NPs in CT26-bearing heterotopic tumor models. (A) Schematic illustration of treatment schedule *in vivo*. (B) Tumor growth curves of CT26-bearing heterotopic tumor models treated with different formulations ($n = 5$). (C) Tumor weights of CT26-bearing heterotopic tumor models treated with different formulations ($n = 5$). Relative expression levels of PD-L1 (D) and CD47 (E) mRNAs in tumor tissues from CT26-bearing heterotopic models treated with different formulations detected using qRT-PCR ($n = 3$). (F) Relative expression levels of PD-L1 and CD47 proteins in tumor tissues from CT26-bearing heterotopic models treated with different formulations detected using Western blot. ELISA analysis of TNF-α (G), IL-6 (H), and IFN-γ (I) concentrations in tumor tissues from CT26-bearing heterotopic models treated with different formulations ($n = 3$). Data represent mean ± S.D. $^{*}P < 0.05$, $^{**}P < 0.01$, and $^{***}P < 0.001$.

free siPD-L1 (25.50%) were all moderately increased (but there was no statistical difference). Lip-Pt/Fu@siPD-L1 NPs group exhibited the highest proportion of tumor-infiltration $CD8^+$ T cells (47.71%), which was 1.4-fold higher than that in the group of the formulation of MiPt plus 5-Fu plus Lip-siPD-L1 (34.9%), and 1.6-fold higher than that in Lip-Pt/Fu@siNC NPs group (30.65%). As shown in Fig. S22B (Supporting information), compared with the control group (53.76%), a lower proportion of regulatory cells (Tregs) was observed in the tumor tissues treated with the different formulations of MiPt (45.32%), MiPt plus 5-Fu (41.11%), MiPt plus 5-Fu plus free siPD-L1 (44.19%), and Lip-Pt/Fu@siNC NPs (41.72%). The lowest proportion of Tregs (30.39%) in the tumor was observed in Lip-Pt/Fu@siPD-L1 NPs group. As shown in Fig. S22C (Supporting information), compared with the control group (16.58%), the proportion of macrophages from the tumor tissues, treated with the formulations of MiPt (24.45%), MiPt plus 5-Fu (25.90%), and MiPt plus 5-Fu plus free siPD-L1 (23.85%) were significantly increased. Lip-Pt/Fu@siPD-L1 NPs group exhibited the highest proportion of macrophages (39.28%), which was 1.5-fold higher than that in the formulation of MiPt plus 5-Fu plus Lip@siPD-L1 group (26.18%), and 1.2-fold higher than that in Lip-Pt/Fu@siNC NPs group (33.75%). The proportions of M1 ($CD86^+$ cells in $F4/80^+CD11b^+$ cells) and M2 ($CD206^+$ cells in $F4/80^+CD11b^+$ cells) macrophages in tumor tissues of each treatment group were showed in Figs. S22D and E (Supporting information). Compared with the control group, the proportion of M1 macrophages from tumor tissues treated with other formulations was increased, and the proportion of M2 macrophages were all reduced. To better evaluate the *in vivo* polarization ability of macrophages induced by each formulation, the ratios of M1/M2 were calculated (Fig. S23 in Supporting information). Compared with the control group (0.42), the M1/M2 ratios of MiPt (0.67), MiPt plus 5-Fu (0.68), and MiPt plus 5-Fu plus free siPD-L1 (0.68) were increased, suggesting that the polarization of macrophage from M2 to M1 was induced by MiPt. The Lip-Pt/Fu@siPD-L1 NPs group exhibited a higher M1/M2 ratio of 0.94 than MiPt, due to its higher accumulation of MiPt in tumor tissues. Moreover, the Lip-Pt/Fu@siNC NPs showed increased expression of CD86 and IL-12 mRNA (the makers of M1 macrophages) and decreased expression of CD206 mRNA (the maker of M2 macrophages) in the tumor tissues when compared with the MiPt group (Figs. S24 and S25 in Supporting information).

Furthermore, the immune cytokines secreted from $CD8^+$ T cells and macrophages in tumor tissues were detected using ELISA kits. As shown in Figs. 4G–I, compared with the control group, the expression levels of tumor necrosis factor-α (TNF-α), interleukin-6 (IL-6), and interferon-γ (IFN-γ) in the tumor tissues treated with different formulations were all increased, and Lip-Pt/Fu@siPD-L1 NPs showed the highest expression level in the above mentioned immune cytokines. Especially for the expression level of IFN-γ, Lip-Pt/Fu@siPD-L1 NPs exhibited 1.4-fold higher than the formulation of MiPt plus 5-Fu plus Lip@siPD-L1, and 1.7-fold higher than Lip-Pt/Fu@siNC NPs. Collectively, these results indicated that Lip-Pt/Fu@siPD-L1 NPs showed the best therapeutic efficacy, rather than the physical mixing of MiPt, 5-Fu and free siPD-L1 (or Lip@PD-L1). It was suggested that Lip-Pt/Fu@siPD-L1 NPs could reshape the tumor microenvironment by improving the intratumoral infiltration of $CD8^+$ T cells and macrophages, promoting macrophage polarization from M2 into M1, depleting Tregs, and elevating immune cytokine secretion.

To evaluate the safety of Lip-Pt/Fu@siPD-L1 NPs *in vivo*, we monitored the body weights of the mice during the treatment, and performed histopathological analysis of major organs at the end of the treatment. As shown in Figs. S26 and S27 (Supporting information), no body weight loss or major organ abnormality was observed in any of the groups. Moreover, no abnormality in the hematological indices (hemoglobin, red blood cell, platelet and

white blood cell) was identified in the Lip-Pt/Fu@siPD-L1 group at the end of the treatment (Fig. S28 in Supporting information).

In summary, we successfully developed MiPt based nanomedicine to assemble with Fu-OA and siPD-L1 into tumor cells for synergistic chemo-immunotherapy. We demonstrated that Lip-Pt/Fu@siPD-L1 NPs could exert significant anti-tumor effects *via* multi-drug synergistic mechanisms. We showed for the first time that Lip-Pt/Fu@siPD-L1 NPs can simultaneously inhibit the expression of CD47 and PD-L1, and exhibit synergistic immunotherapeutic effects on tumor growth, which include the enhancement of intratumoral infiltration of macrophages and the proportion of M1 macrophages, improvement of intratumoral infiltration of $CD8^+$ T cells, depletion of Tregs and elevation of immunostimulatory cytokine secretion. Such an integrated multi-drug delivery system could provide a potential strategy for tumor chemo-immunotherapy.

Declaration of competing interest

The authors declare that they have no known competing financial interests or personal relationships that could have appeared to influence the work reported in this paper.

Acknowledgments

The authors acknowledge financial support from the Basic Research Cooperation Project of Beijing, Tianjin, Hebei from the Natural Science Foundation of Beijing (No. J200018), Tianjin (No. 20JCZXJC00070), and Hebei (No. H2020206649), Beijing Natural Science Foundation (No. 7214281), and the projects of National Natural Science Foundation of China (No. 81973259).

Supplementary materials

Supplementary material associated with this article can be found, in the online version, at doi:10.1016/j.cclet.2023.108928.

References

[1] R. Zhang, X.Q. Song, R.P. Liu, Z.Y. Ma, J.Y. Xu, J. Med. Chem. 62 (2019) 4543–4554.
[2] T.A. Seidu, P.T. Kutoka, D.O. Asante, et al., Pharmaceutics 14 (2022) 1113.
[3] R.G. Kenny, C.J. Marmion, Chem. Rev. 119 (2019) 1058–1137.
[4] Y. Shi, Z. Zhao, K. Peng, et al., Adv. Healthc. Mater. 10 (2021) e2001455.
[5] Y. Tian, Q. Zhao, Y. Li, et al., Gastroenterol. Res. Pract. 2021 (2021) 5590626.
[6] X. Sun, Y. Wang, T. Du, et al., Chin. Chem. Lett. 34 (2023) 108201.
[7] H. Nasrolahi, S. Mirzaei, M. Mohammadianpanah, et al., Ann. Coloproctol. 35 (2019) 242–248.
[8] L. Fournel, Z. Wu, N. Stadler, et al., Cancer Lett. 464 (2019) 5–14.
[9] E. Bockamp, S. Rosigkeit, D. Siegl, D. Schuppan, Cells 9 (2020) 2102.
[10] L. Zhou, M. Zou, Y. Xu, et al., Front. Oncol. 12 (2022) 864301.
[11] L. Zhai, Y. Shi, Y. Yan, et al., Chin. Chem. Lett. 34 (2023) 108104.
[12] Y.S. Harada, K. Kato K, Future Oncol. 18 (2022) 2311–2319.
[13] A. Abed, M. Derakhshan, M. Karimi, et al., Front. Pharmacol. 13 (2022) 797804.
[14] Y. Xue, S. Gao, J. Gou, et al., Expert Opin. Drug Deliv. 18 (2021) 187–203.
[15] V. Novohradsky, J. Pracharova, J. Kasparkova, et al., Inorg. Chem. Front. 7 (2020) 4150–4159.
[16] X. Huang, L. Han, R. Wang, et al., Drug Deliv. 29 (2022) 1358–1369.
[17] J. Guo, Z. Yu, M. Das, L. Huang, ACS Nano 14 (2020) 5075–5089.
[18] J. Guo, Z. Yu, D. Sun, et al., Mol. Cancer 20 (2021) 10.
[19] Y. Zhang, D. Hu, S. Han, et al., Exp. Biol. Med. 241 (2016) 1169–1176.
[20] S. Liu, Y. Li, X. Wang, et al., J. Pharm. Sci. 105 (2016) 78–87.
[21] X. Kang, H.H. Xiao, H.Q. Song, et al., Cancer Biol. Med. 12 (2015) 362–374.
[22] A.G. Niculescu, A.M. Grumezescu, Int. J. Mol. Sci. 23 (2022) 5253.
[23] Y. Shi, A. Lu, X. Wang, et al., Acta Pharm. Sin. B 11 (2021) 2396–2415.
[24] X. Ling, W. Han, X. Jiang, et al., Biomaterials 270 (2021) 120690.
[25] J. Zuo, X. Gao, J. Xiao, Y. Cheng, Chin. Chem. Lett. 34 (2023) 107827.
[26] R. Zhang, G. Cheng, S. Liu, H. Lv, J. Li, J. Mater. Chem. B 9 (2021) 8809–8822.
[27] Y. Yan, A. Lu, Y. Dou, et al., Adv. Sci. 10 (2023) e2207490.